NACA

RESEARCH MEMORANDUM

for the

Bureau of Aeronautics, Department of the Navy

STATIC LONGITUDINAL AND LATERAL STABILITY AND CONTROL CHARACTERISTICS OF A 1/15-SCALE MODEL OF THE GRUMMAN F9F-9 AIRPLANE AT A MACH NUMBER OF 1.41

TED NO. NACA DE 390

By Edward B. Palazzo and M. Leroy Spearman

Langley Aeronautical Laboratory
Langley Field, Va.

NATIONAL ADVISORY COMMITTEE
FOR AERONAUTICS

WASHINGTON
JUL 14 1954

NATIONAL ADVISORY COMMITTEE FOR AERONAUTICS

RESEARCH MEMORANDUM

for the

Bureau of Aeronautics, Department of the Navy

STATIC LONGITUDINAL AND LATERAL STABILITY AND CONTROL CHARACTERISTICS OF A 1/15-SCALE MODEL OF THE GRUMMAN F9F-9 AIRPLANE AT A MACH NUMBER OF 1.41

TED NO. NACA DE 390

By Edward B. Palazzo and M. Leroy Spearman

SUMMARY

An investigation has been conducted in the Langley 4- by 4-foot supersonic pressure tunnel at a Mach number of 1.41 to determine the static stability and control and drag characteristics of a 1/15-scale model of the Grumman F9F-9 airplane. The effects of alternate fuselage shapes, wing camber, wing fences, and fuselage dive brakes on the aerodynamic characteristics were also investigated. These tests were made at a Reynolds number of 1.96×10^6 based on the wing mean aerodynamic chord of 0.545 foot.

The basic configuration had a static margin of stability of 38.4 percent of the mean aerodynamic chord and a minimum drag coefficient of 0.049. For the maximum horizontal tail deflection investigated (-10°), the maximum trim lift coefficient was 0.338. The basic configuration had positive static lateral stability at zero angle of attack and positive directional control throughout the angle-of-attack range investigated up to 11°.

INTRODUCTION

At the request of the Bureau of Aeronautics, Department of the Navy, an investigation of the aerodynamic characteristics of the Grumman F9F-9

airplane at subsonic, transonic, and low supersonic speeds has been undertaken by the National Advisory Committee for Aeronautics.

This airplane is a jet-propelled day-fighter design having a wing with 35° sweep at the quarter-chord line, an aspect ratio of 4, and a thickness ratio of 6 percent at the root and 4 percent at the tip. The wing is mounted in a semihigh position on the fuselage and an all-movable horizontal tail is located slightly below the extended chord line of the wing. The fuselage is indented in the vicinity of the wing in an effort to obtain a desirable area distribution for the purpose of reducing the transonic drag rise.

Tests have been conducted at subsonic speeds in the Langley low-turbulence pressure tunnel (unpublished) and through the transonic range in the Langley 8-foot transonic tunnel (unpublished). The present paper contains the results obtained at a Mach number of 1.41 in the Langley 4- by 4-foot supersonic pressure tunnel.

COEFFICIENTS AND SYMBOLS

In the presentation of the experimental results, the force and moment coefficients are referred to the stability axis system with the reference center-of-gravity location (center of moments) at the 25 percent point of the mean aerodynamic chord.

C_L lift coefficient, $\frac{\text{Lift}}{qS}$

C_X longitudinal-force coefficient (C_X is positive forward), $\frac{\text{Longitudinal force}}{qS}$

C_m pitching-moment coefficient, $\frac{\text{Pitching moment}}{qS\bar{c}}$

C_l rolling-moment coefficient, $\frac{\text{Rolling moment}}{qSb}$

C_n yawing-moment coefficient, $\frac{\text{Yawing moment}}{qSb}$

C_Y lateral-force coefficient, $\frac{\text{Lateral force}}{qS}$

S wing area, sq ft

q dynamic pressure, lb/sq ft

$\bar{c}$ wing mean aerodynamic chord, ft

M free-stream Mach number

L/D lift-drag ratio $\left(C_L/-C_X \text{ for } \beta = 0^\circ\right)$

R Reynolds number

b wing span, ft

α angle of attack of fuselage reference line, deg

β angle of sideslip, deg

i_t stabilizer incidence angle with respect to fuselage center line (positive when trailing edge moves down), deg

δ_r rudder deflection in streamwise direction (positive when trailing edge moves to left), deg

ϵ effective downwash angle, deg

MODEL DESIGNATIONS

W wing (subscript S denotes symmetrical section; subscript C denotes cambered leading edge)

B body (subscript 1 denotes standard fuselage; subscript 2 denotes fuselage with revised indentation)

V vertical tail

H horizontal tail

Z fence

MODEL AND APPARATUS

The tests were conducted in the Langley 4- by 4-foot supersonic pressure tunnel at a Mach number of 1.41. The 1/15-scale model of the Grumman F9F-9 used in this investigation is shown in figure 1 and its geometric characteristics are presented in table I. Photographs of the model are shown in figure 2.

The basic configuration for this investigation had a wing with 35° sweepback at the quarter-chord line and an NACA 65A006 section at the root and an NACA 65A004 section at the tip that was modified to incorporate a cambered leading edge. The wing had a taper ratio of 0.5, an aspect ratio of 4, and was mounted in a semihigh position on the fuselage. An all-movable horizontal tail was mounted below the extended chord plane of the wing. A substantial part of the longitudinal area distribution resulting from the wing was removed by indentation of the sides of the fuselage.

Two differently indented fuselage shapes, B_1 and B_2 (see fig. 1), were used in this investigation. The maximum indentation for B_2 was farther forward than that for B_1. The model was equipped with a rudder, chordwise wing fences, dive brakes, and conventional subsonic twin side inlets. For most of the tests the inlets were open to permit air flow through the ducts. For a few tests faired plugs were used to close the inlets so that some results might be obtained without flow through the ducts. The internal flow characteristics for the configurations having open inlets were determined through the use of a rake placed at the duct exit (see fig. 2) for the purpose of measuring the total and static pressures. Pressure measurements were made with the rake placed in two positions located 45° apart so that a greater area of the duct exit might be surveyed. The rake was removed for those tests in which forces and moments were measured.

The leading edge of the wing could be removed and an alternate leading edge installed. Two leading edges were investigated: one symmetrical and the other cambered. Coordinates for the wing with different leading edges are presented in table II. The basic model configuration utilized the cambered leading edge.

Forces and moments were measured by means of a six-component internal strain-gage balance.

TESTS

Test Conditions

The tests were conducted at a Mach number of 1.41, a stagnation pressure of 12 pounds per square inch, and a stagnation temperature of 100° F. The dewpoint was maintained at -25° F or less to prevent adverse condensation effects.

The Reynolds number based on a mean aerodynamic chord of 0.545 foot was 1.96×10^6. The dynamic pressure for the test was about 750 pounds per square foot.

Corrections and Accuracy

The angles of attack and sideslip have been corrected for deflections of the balance and sting caused by the aerodynamic loads.

Base pressure measurements were made and the longitudinal-force coefficients were corrected to correspond to a base pressure equal to free-stream static pressure. The model internal pressure was measured and corrections for a buoyant force on the balance have also been applied to the drag results. Internal drag as determined from average pressures obtained from the rake measurements was subtracted for the open duct configurations so that a net external drag was obtained. Except where noted otherwise, all tests were made with air flow through the ducts. For the open-duct configurations, a mass-flow ratio of about 0.7 was indicated and the internal longitudinal-force coefficient was about -0.005.

The angles of attack, sideslip, and control deflection are estimated to be accurate to within ±0.1°. Mach number variation in the test section was approximately ±0.01.

The maximum estimated errors in the coefficients due to the balance system are as follows:

C_L	±0.007
C_X	±0.001
C_m	±0.005
C_l	±0.0003
C_n	±0.0001
C_Y	±0.001

PRESENTATION OF RESULTS

Aerodynamic Characteristics in Pitch

Longitudinal stability and control of basic configuration.- The aerodynamic characteristics in pitch for the complete configuration with cambered wing and open ducts $(W_C B_1 ZVH)$ with various values of tail incidence angle as well as with the horizontal tail off are presented in figure 3.

The slopes of the pitching-moment curves (fig. 3) indicate a static margin of $0.384\bar{c}$ or a neutral-point location at 63.4 percent of $\bar{c}$. Location of the aerodynamic center for the tail-off configuration is about 42.5 percent of $\bar{c}$.

The lift-curve slope C_{L_α} is about 0.079 for the complete model with $i_t = 0^\circ$. The corresponding minimum longitudinal-force coefficient is -0.049. The variation of longitudinal force due to lift (fig. 4) indicates a value of $\Delta C_X / C_L{}^2$ of about 0.233 as compared to the reciprocal of the lift-curve slope $\left(\frac{1}{57.3 C_{L_\alpha}}\right)$ of 0.221.

The pitching effectiveness of the tail as defined by the parameter $\partial C_m / \partial i_t$ (fig. 5) is about -0.015 and remains essentially constant with angle of attack. These data were used in conjunction with the tail-off pitching moments to obtain the variation of effective downwash angle with angle of attack from the relation $\epsilon = \alpha + i_t$ at the point of intersection of a tail-on and tail-off pitching-moment curve (fig. 5). The resulting value of $\partial \epsilon / \partial \alpha$ is about -0.16. From the position of the wing tip Mach cones with respect to the horizontal tail at $M = 1.41$, it might be expected that the wing has only a small effect on the flow angularity at the tail and that the effective upwash results primarily from the upwash field of the body. This effective upwash serves to increase the static longitudinal stability.

Trim longitudinal stability and control characteristics (fig. 6) indicate that, for the maximum horizontal tail deflection investigated (-10°), $C_{L_{max}}$ was about 0.338 with a trim C_X of -0.085 and a trim L/D of about 4. The minimum trim value of C_X is about -0.049 with a lift-curve slope C_{L_α} of 0.061 in the low lift range.

Effect of air flow through inlets and fixed transition.- A comparison of the results obtained for the complete model $(W_C B_1 ZVH)$ with ducts

open and closed and with transition fixed by applying roughness to the body nose and wing leading edges indicates little difference in the longitudinal characteristics (fig. 7).

Effect of body shape.- The revised body (B_2) in comparison with the basic body (B_1) for the model with inlets both open and closed and with the horizontal tail removed (W_CBZV) indicates no significant change in minimum C_X, but a slightly higher C_{L_α} and a slightly lower increase in longitudinal force with increasing lift. (See fig. 8.)

Effect of wing section.- A comparison of the symmetrical wing section with the cambered wing section for the model with the inlets open and with the horizontal tail both on and off (fig. 9) indicates for the cambered wing a slightly higher minimum longitudinal-force coefficient and slightly less variation of longitudinal-force coefficient with lift coefficient. In addition, the effect of camber was to increase slightly the lift-curve slope and cause a reduction in the trim lift coefficient.

Effect of wing fences.- The addition of wing fences to the basic configuration either with or without the horizontal tail (fig. 10) apparently had little effect on the longitudinal characteristics except for a slight increase in the minimum C_X.

Effect of dive brakes.- The addition of dive brakes to the configuration with or without the horizontal tail (fig. 11) results in an incremental increase in C_X of 0.059 at an angle of attack of 0°. For the model with the tail on, there was little change in the stability $\left(\partial C_m/\partial C_L\right)$ as a result of deflecting the brakes but the trim lift coefficient was decreased about 0.06 and the angle of attack for zero lift was decreased about 1.5°.

Aerodynamic Characteristics in Sideslip

Lateral stability characteristics for basic configuration.- The aerodynamic characteristics in sideslip for the complete model (W_CB_1ZVH) at $\alpha = 0^\circ$ and $i_t = 0^\circ$ (fig. 12) indicate positive static lateral and directional stability. The lateral stability derivatives are summarized in the following table:

	Derivative for -		
	$\delta_r = 0^\circ$	Trim ($C_n = 0$)	Tail-off
C_{l_β}	-0.00124	-0.00055	0
C_{n_β}	0.0019	--------	-0.0024
C_{Y_β}	-0.0135	-0.010	-0.0042

The derivatives for trim ($C_n = 0$) were estimated assuming that the variation of C_l, C_n, and C_Y with β for δ_r of 5° and 10° were parallel to those obtained for $\delta_r = 0^\circ$. It is interesting to note that the effective dihedral $\left(C_{l_\beta}\right)$ for the complete model is contributed entirely by the vertical tail and hence might be expected to be influenced by deflections of the rudder. The resulting C_{l_β} for trimmed sideslip (wherein the rudder is deflected to maintain steady sideslip) is less than one-half that for the model with the rudder fixed at zero deflection.

It should be pointed out that the lateral characteristics were measured at a slightly negative C_L and the derivatives may vary somewhat for other lift coefficients. In particular, the slope C_{n_β} might be expected to decrease with increasing C_L. The variation of effective dihedral with lift coefficient $C_{l_{\beta C_L}}$, however, is less predictable since for $M = 1.41$ the wing leading edge is slightly supersonic and it may be expected that the value of $C_{l_{\beta C_L}}$ for the isolated wing would change from negative to positive at the Mach number for which the Mach line lies along the wing leading edge. (See ref. 1.) In addition, the presence of the vertical tail, wing geometric dihedral, and wing-body interference would influence $C_{l_{\beta C_L}}$.

Directional control characteristics.- The variations of the lateral characteristics with rudder deflection at $\alpha = 0^\circ$ (fig. 13) as obtained from (fig. 12) indicate positive directional control. The directional control characteristics are as follows:

$C_{l_{\delta_r}} = 0.00028$ $\qquad$ $C_{n_{\delta_r}} = -0.00067$

$C_{Y_{\delta_r}} = 0.001$ $\qquad$ $\beta_{\delta_r} = 0.39$

Varying the angle of attack up to about 11° at $\beta = 0°$ had little effect on the slopes $C_{l_{\delta_r}}$, $C_{Y_{\delta_r}}$, or $C_{n_{\delta_r}}$ (fig. 14).

CONCLUSIONS

An investigation of a 1/15-scale model of the Grumman F9F-9 airplane at a Mach number of 1.41 indicated the following conclusions:

1. A high degree of longitudinal stability was obtained that was aggravated to some extent by an effective upwash at the tail.

2. The maximum trim lift coefficient obtained with a maximum horizontal-tail deflection of -10° was 0.338 with a trim longitudinal-force coefficient of -0.085 and a resulting trim L/D of about 4.

3. The minimum longitudinal-force coefficient with a horizontal-tail deflection of 0° was -0.049.

4. The configuration indicated positive directional stability and positive effective dihedral at zero angle of attack.

5. Positive directional control was indicated throughout the angle of attack range up to about 11° with a value of β_{δ_r} of about 0.39 at $\alpha = 0°$.

Langley Aeronautical Laboratory,
National Advisory Committee for Aeronautics,
Langley Field, Va., June 23, 1954.

Edward B. Palazzo /mls

Edward B. Palazzo
Aeronautical Engineer

M. Leroy Spearman

M. Leroy Spearman
Aeronautical Research Scientist

Approved:

John V. Becker
Chief of Compressibility Research Division

ecc

REFERENCE

1. Jones, Arthur L., and Alksne, Alberta: A Summary of Lateral-Stability Derivatives Calculated for Wing Plan Forms in Supersonic Flow. NACA Rep. 1052, 1951.

TABLE I.- GEOMETRIC CHARACTERISTICS OF MODEL

Wing:	
Area, sq ft	1.11
Aspect ratio	4
Sweepback of quarter-chord line, deg	35
Taper ratio	0.5
Mean aerodynamic chord, ft	0.5453
Airfoil section, root	NACA 65A006
Airfoil section, tip	NACA 65A004
Twist, deg	0
Dihedral	2° 30'
Span, ft	2.109
Incidence, deg	0
Horizontal tail:	
Area, sq ft	0.139
Aspect ratio	4
Sweepback of quarter-chord line, deg	35
Taper ratio	0.25
Airfoil section, root	NACA 65A006
Airfoil section, tip	NACA 65A004
Span, ft	1.054
Vertical tail:	
Area (exposed), sq ft	0.154
Aspect ratio (based on exposed area and span)	2.96
Sweepback of leading edge, deg	50
Taper ratio	0.2
Airfoil section, root (2.268 in. above fuselage reference line)	NACA 65A006
Airfoil section, tip	NACA 65A004
Fuselage:	
Length, ft	2.561
Miscellaneous:	
Tail length from $\bar{c}/4$ wing to $\bar{c}_t/4$ tail, ft	0.829
Base area, sq in.	4.48

TABLE II.- WING COORDINATES FOR SYMMETRICAL AND CAMBERED LEADING EDGE

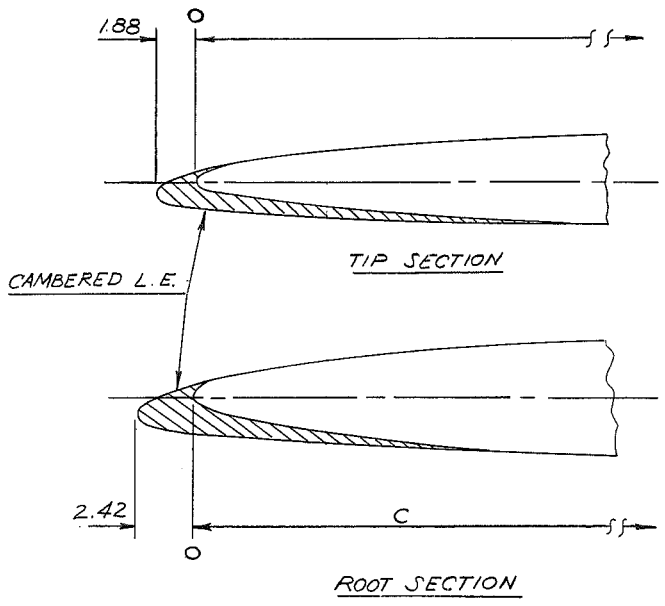

X	Cambered L.E. modification				Symmetrical L.E.	
	Root 65A006 modified		Tip 65A004 modified		Tip 65A004	Root 65A006
	Y_U	Y_L	Y_U	Y_L	Y	Y
-2.42	Vert. tan.	To L.E. rad.			0	0
-2.00	-0.475	-1.510			.50	.311	.464
-1.88			Vert. tan.	To L.E. rad.	.75	.378	.563
-1.54			-0.550	-1.360	1.25	.481	.718
-1.25	-.070	-1.730	-.395	-1.435	2.5	.656	.981
-.75	.145	-1.815	-.200	-1.495	5.0	.877	1.313
-.50	.245	-1.850	-.150	-1.460	7.5	1.062	1.591
0	.415	-1.915	.010	-1.535	10	1.216	1.824
.50	.565	-1.975	.130	-1.560	15	1.463	2.194
.75	.630	-2.005	.175	-1.570	20	1.649	2.474
1.25	.750	-2.060	.270	-1.590	25	1.790	2.687
2.5	.990	-2.190	.455	-1.640	30	1.894	2.842
5.0	1.330	-2.380	.710	-1.735	35	1.962	2.945
7.5	1.595	-2.495	.925	-1.800	40	1.996	2.996
10	1.824	-2.580	1.095	-1.845	45	1.996	2.992
15	2.194	-2.700	1.380	-1.880	50	1.952	2.925
20	2.474	-2.805	1.590	-1.910	55	1.867	2.793
25	2.687	-2.880	1.760	-1.940	60	1.742	2.602
30	2.842	-2.945	1.880	-1.965	65	1.584	2.364
35	2.945	-2.985	1.970	-1.995	70	1.400	2.087
40	2.996	-2.996	1.996	-1.996	75	1.193	1.775
45	2.992	-2.992	1.996	-1.996	80	.966	1.437
50	2.925	-2.925	1.952	-1.952	85	.728	1.083
55	2.793	-2.793	1.867	-1.867	90	.490	.727
60	2.602	-2.602	1.742	-1.742	95	.249	.370
65	2.364	-2.364	1.584	-1.584	100	.009	.013
70	2.087	-2.087	1.400	-1.400	L.E. rad.	.102	.229
75	1.775	-1.775	1.193	-1.193	T.E. rad.	.010	.014
80	1.437	-1.437	.966	-.996			
85	1.083	-1.083	.728	-.728			
90	.727	-.727	.490	-.490			
95	.370	-.370	.249	-.249			
100	0	0	.009	-.009			

Note: Coordinates read from basic airfoil chord line:

L.E. radius of 6-percent section = 0.250 at X = -2.17, Y = -1.06
T.E. radius of 6-percent section = 0.014
L.E. radius of 4-percent section = 0.340 at X = -1.54, Y = -0.99
T.E. radius of 4-percent section = 0.010

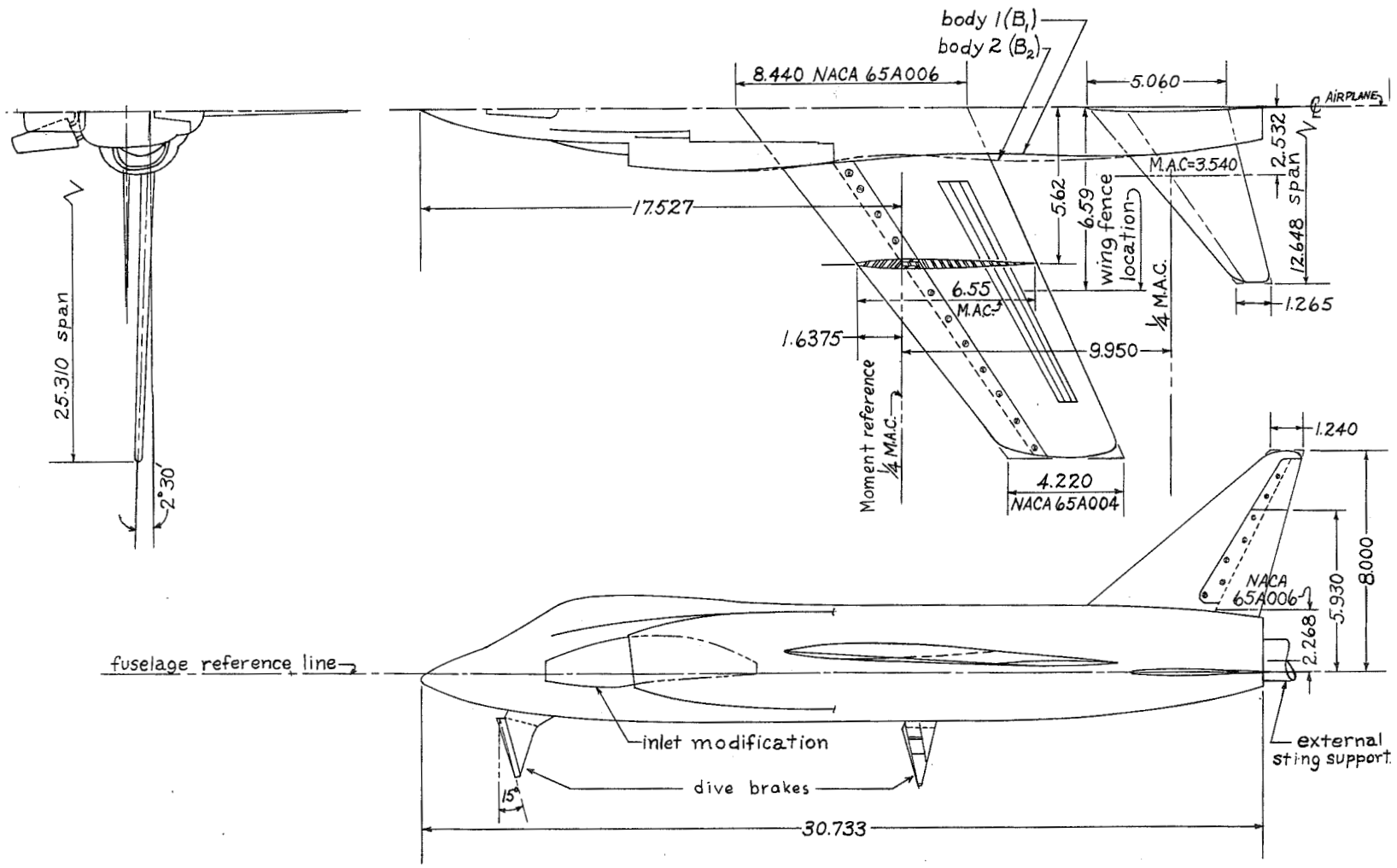

Figure 1.- Drawing of 1/15-scale Grumman F9F-9 model. All dimensions in inches.

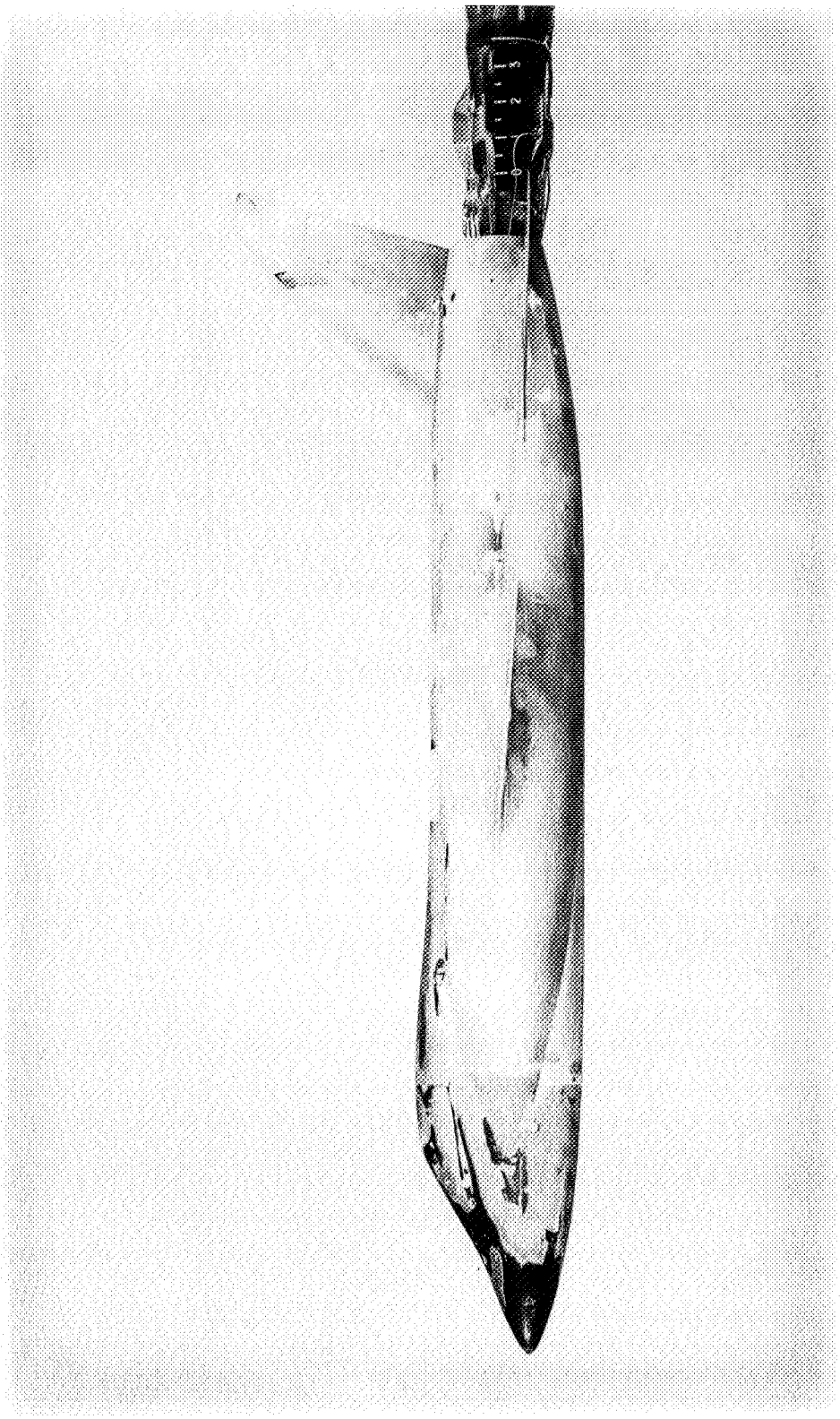

L-82214

Figure 2.- Photographs of model.

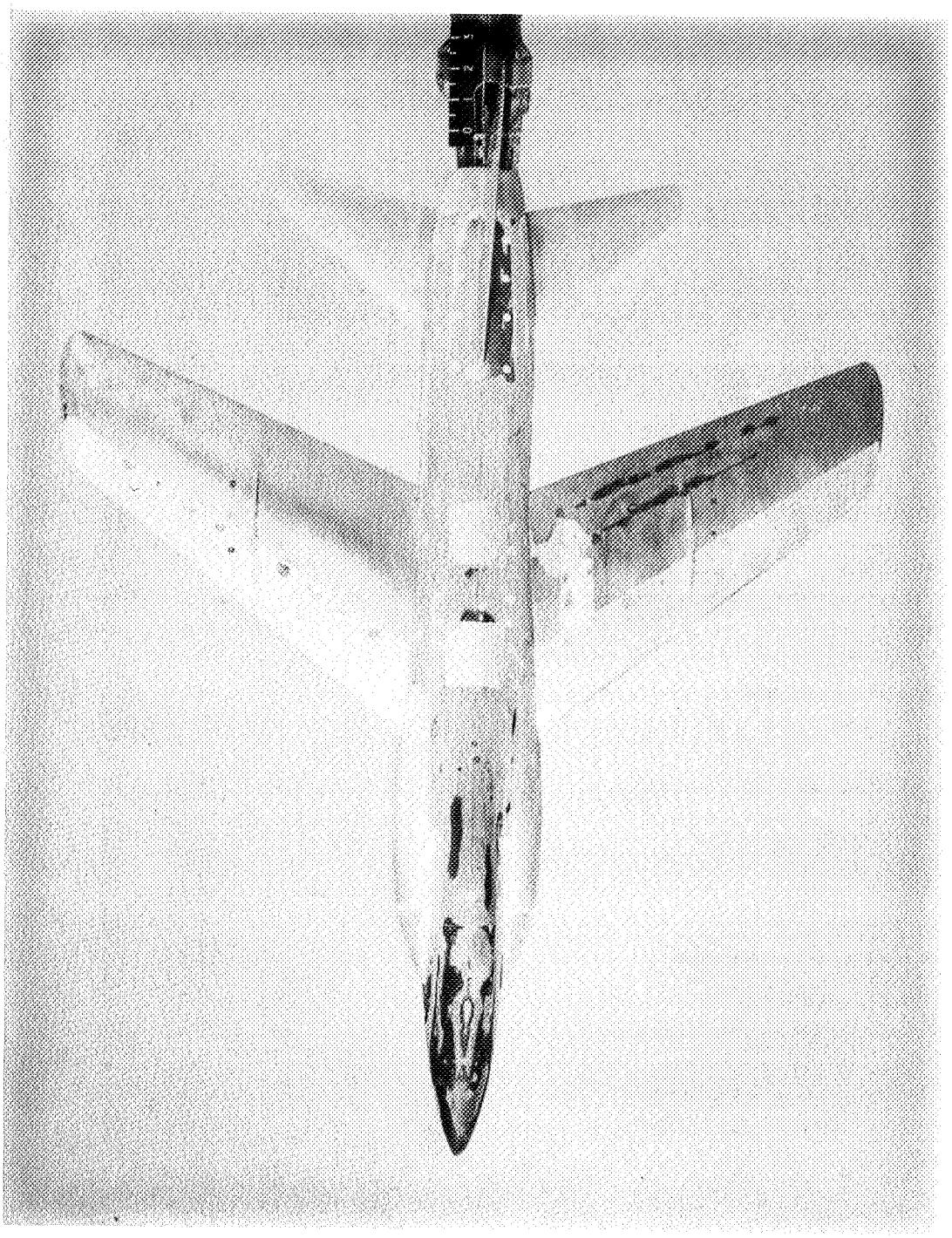

L-82215

Figure 2.- Concluded.

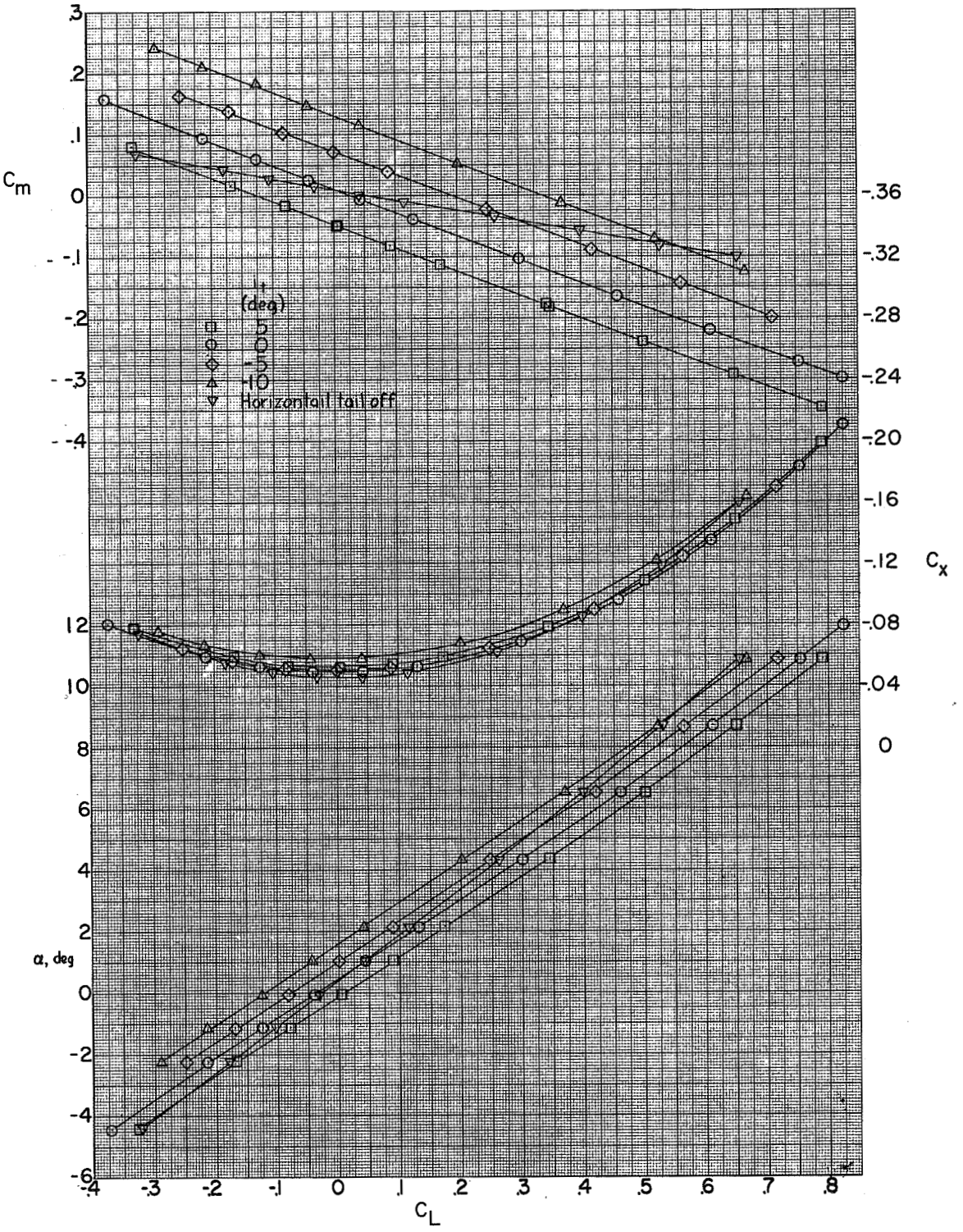

Figure 3.- Effect of horizontal tail on the aerodynamic characteristics in pitch. Configuration $W_C B_1 ZVH$; inlets open.

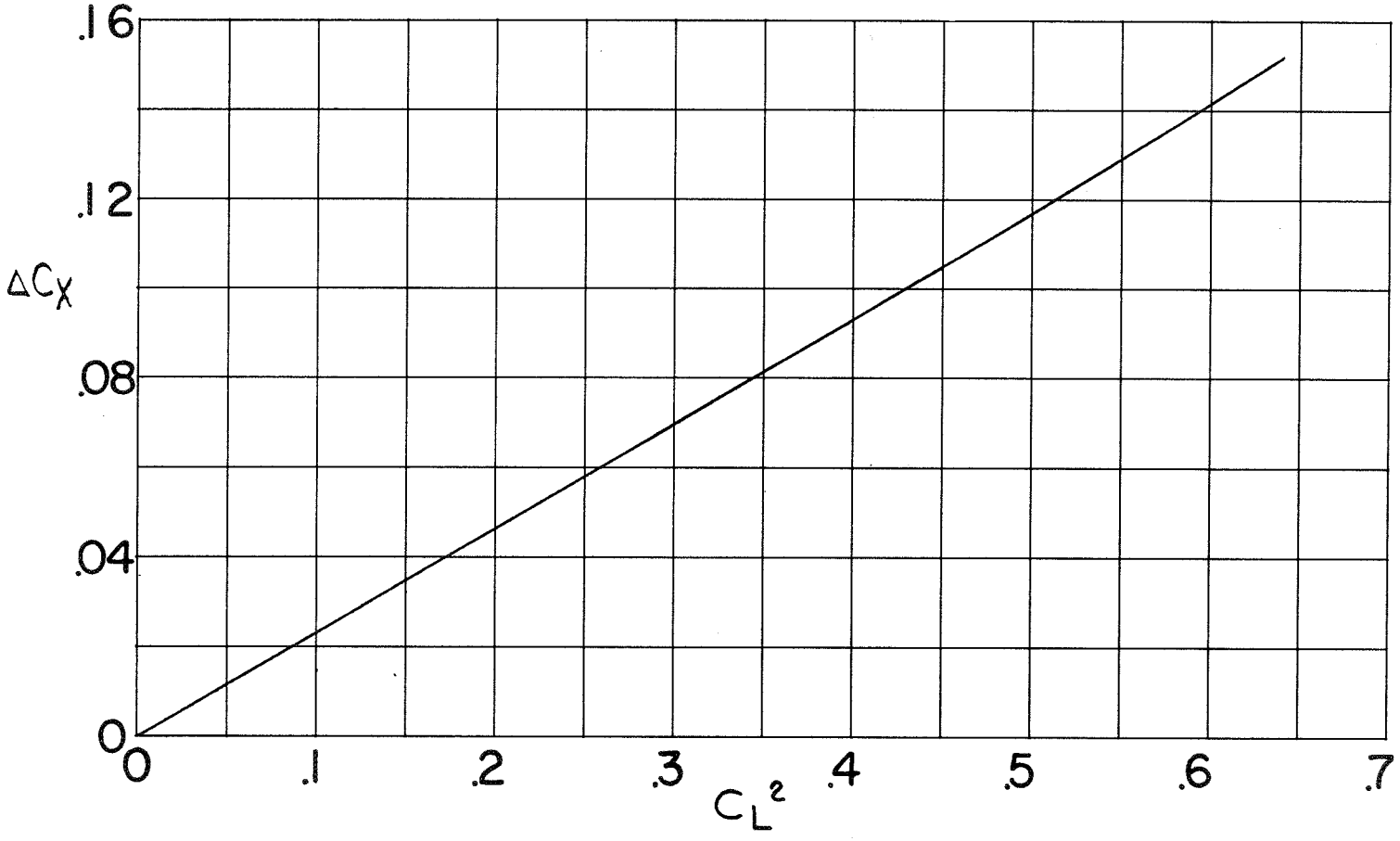

Figure 4.- Variation of longitudinal force due to lift.
Configuration $W_C B_1 ZVH$; inlets open; $i_t = 0^\circ$.

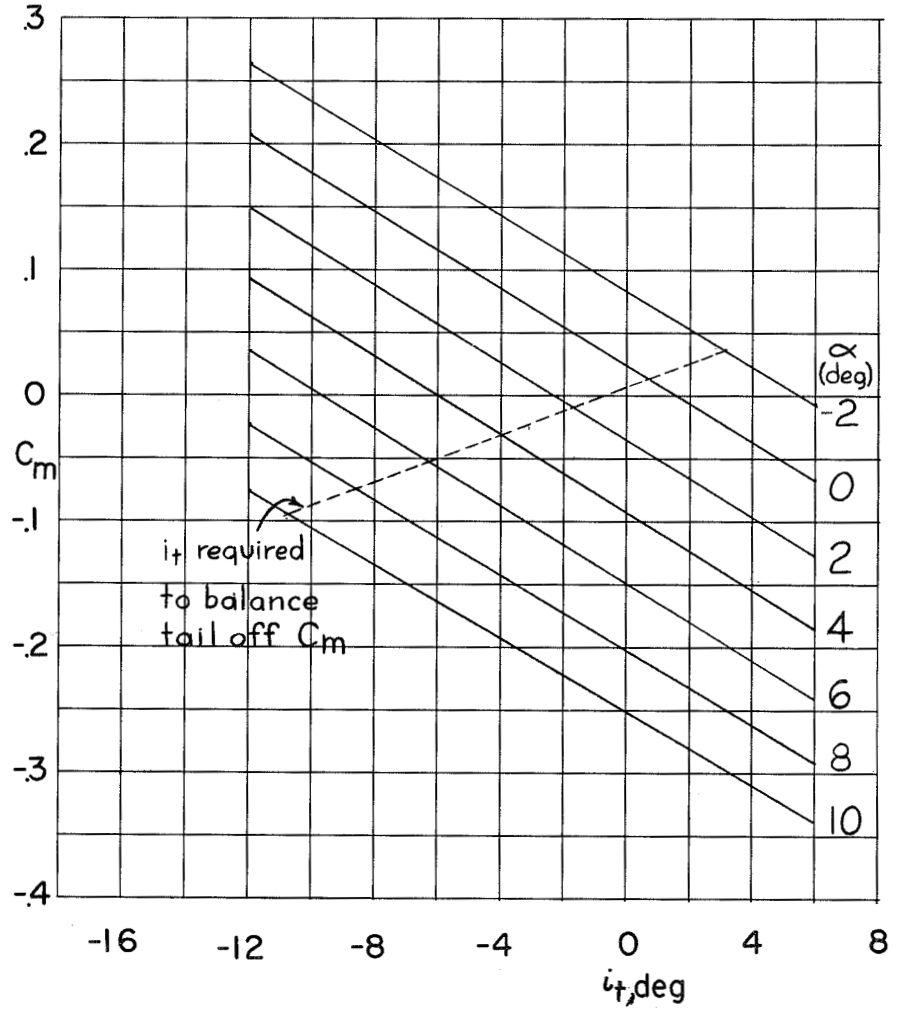

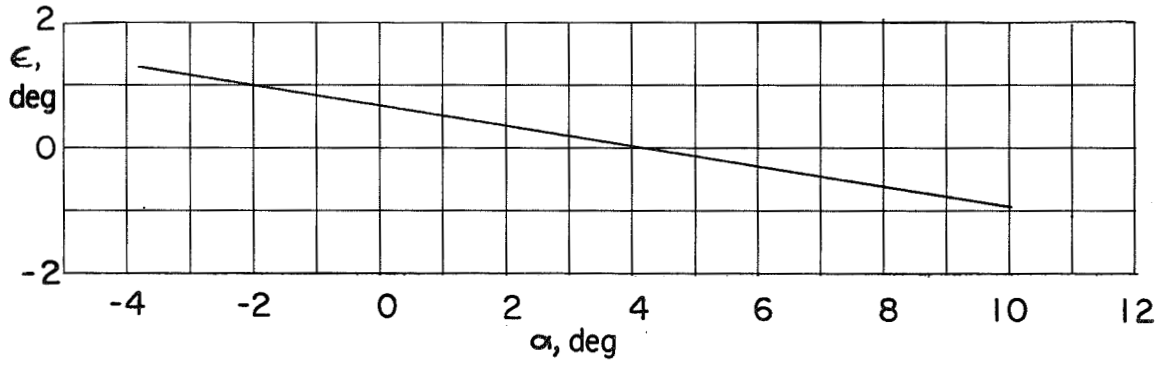

Figure 5.- Tail pitching effectiveness and effective downwash characteristics. Inlets open.

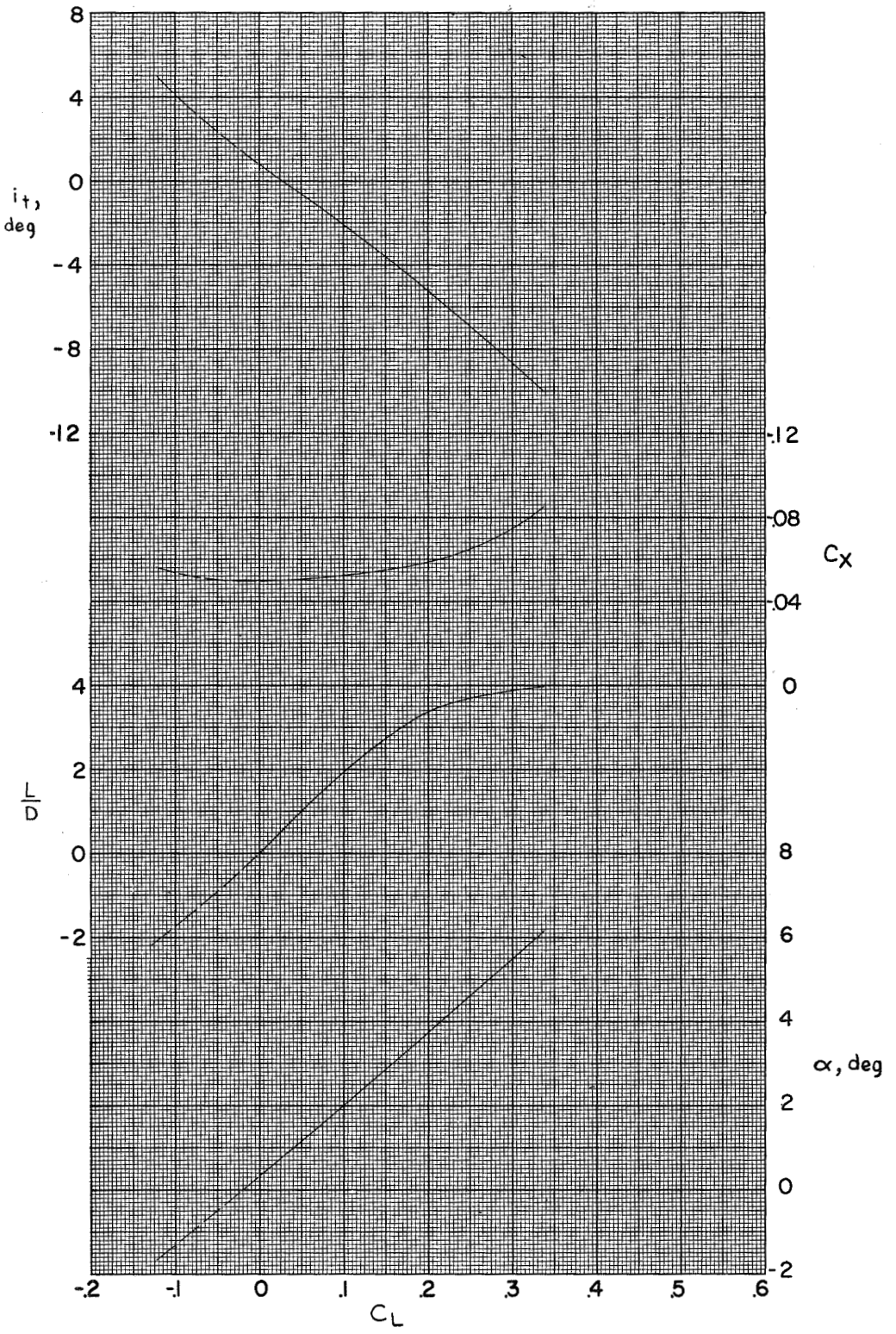

Figure 6.- Variation of trim longitudinal characteristics with lift coefficient. Inlets open; $C_m = 0$.

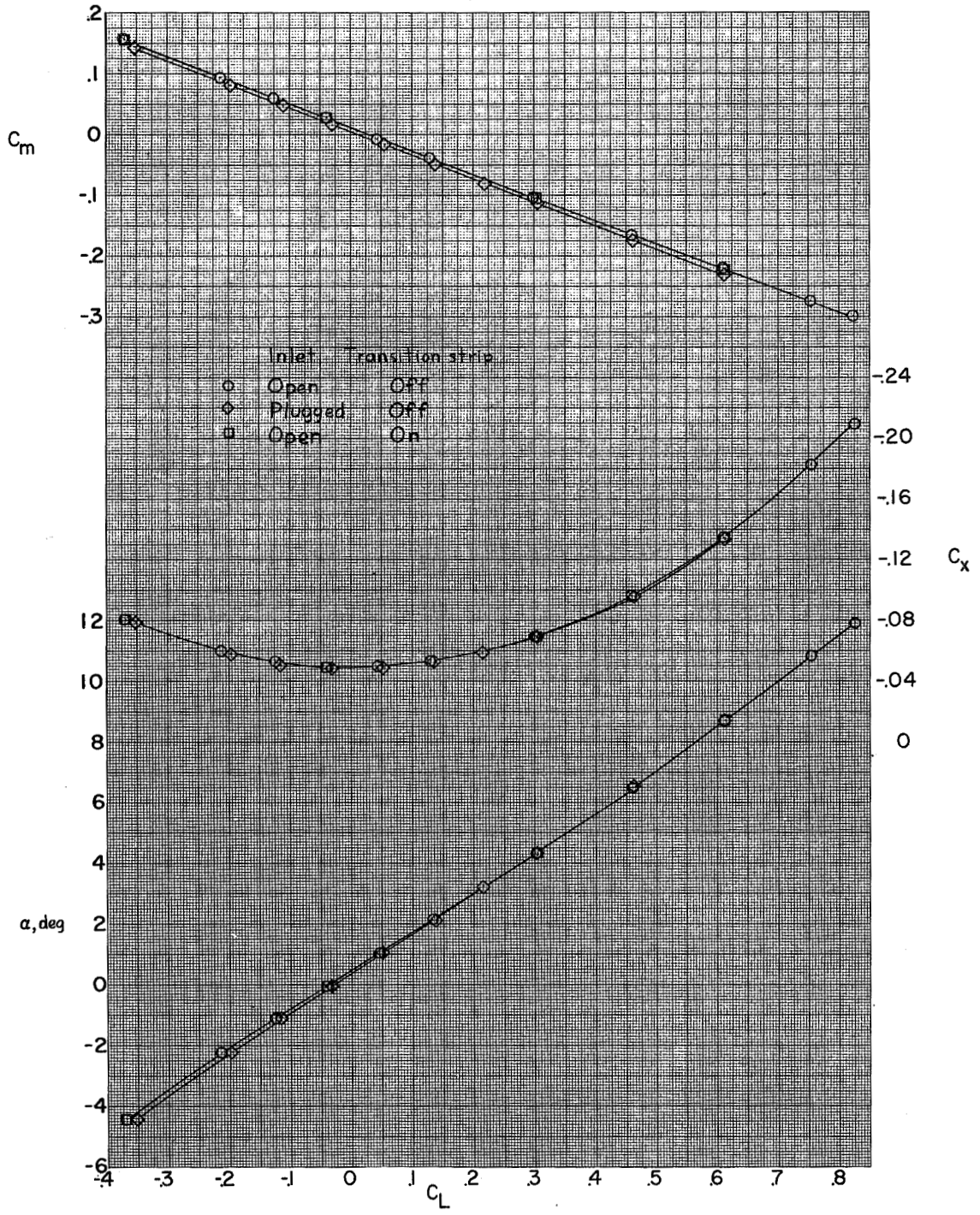

Figure 7.- Effect of closing inlet and of fixing transition on aerodynamic characteristics in pitch. Configuration $W_C B_1 ZVH$; $i_t = 0^o$.

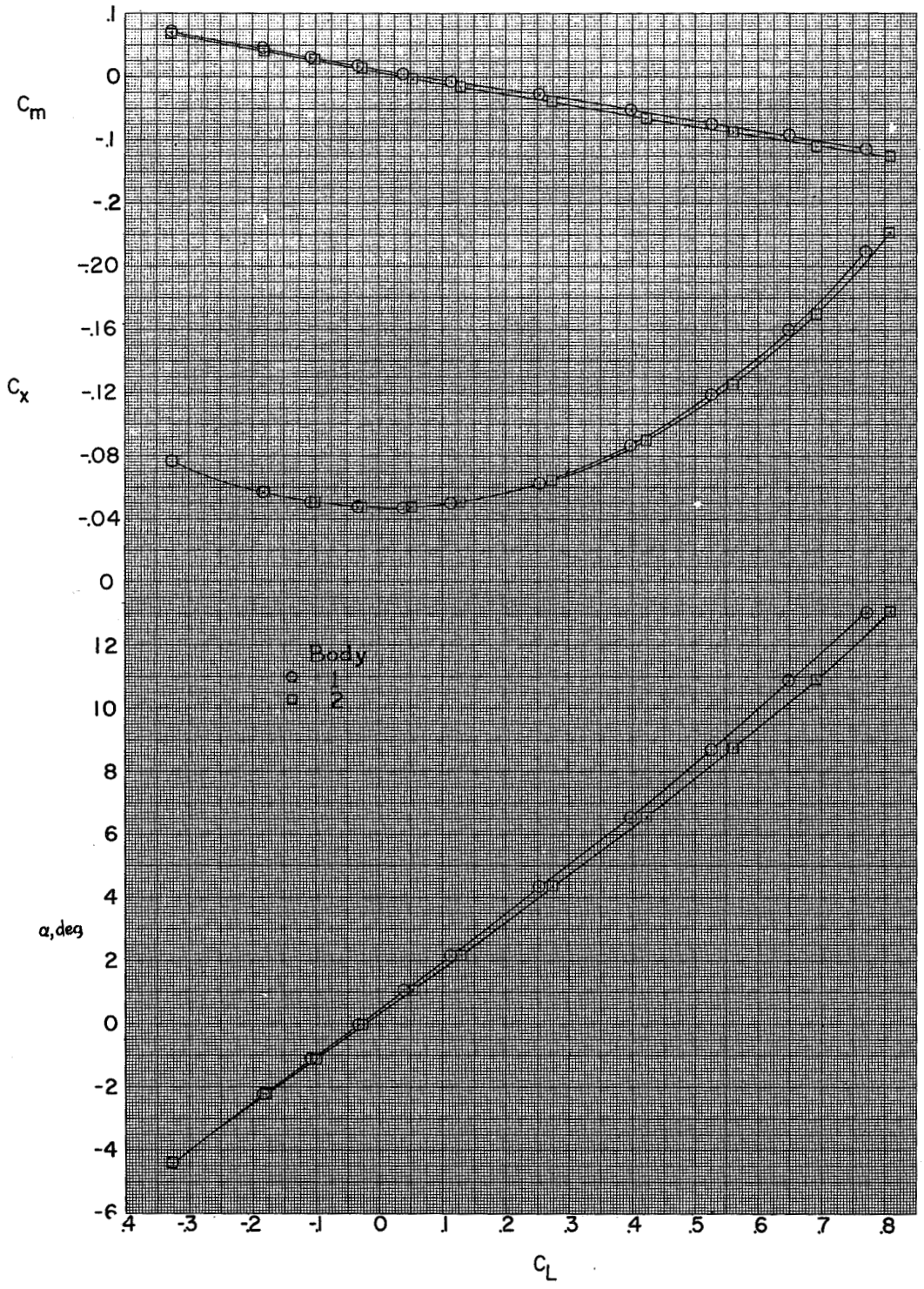

(a) Inlet open.

Figure 8.- Effect of body shape on aerodynamic characteristics in pitch. Horizontal tail off.

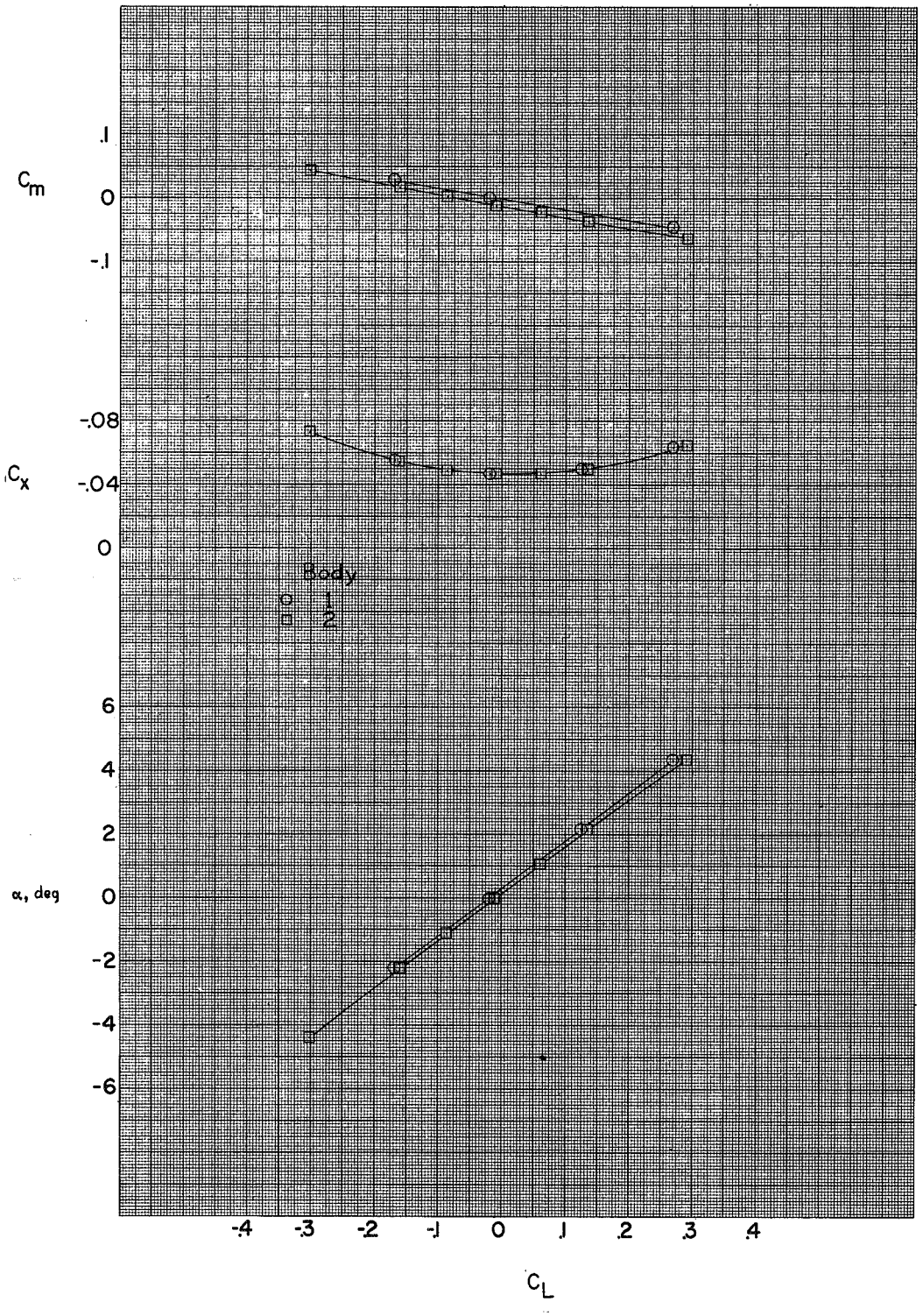

(b) Inlet closed.

Figure 8.- Concluded.

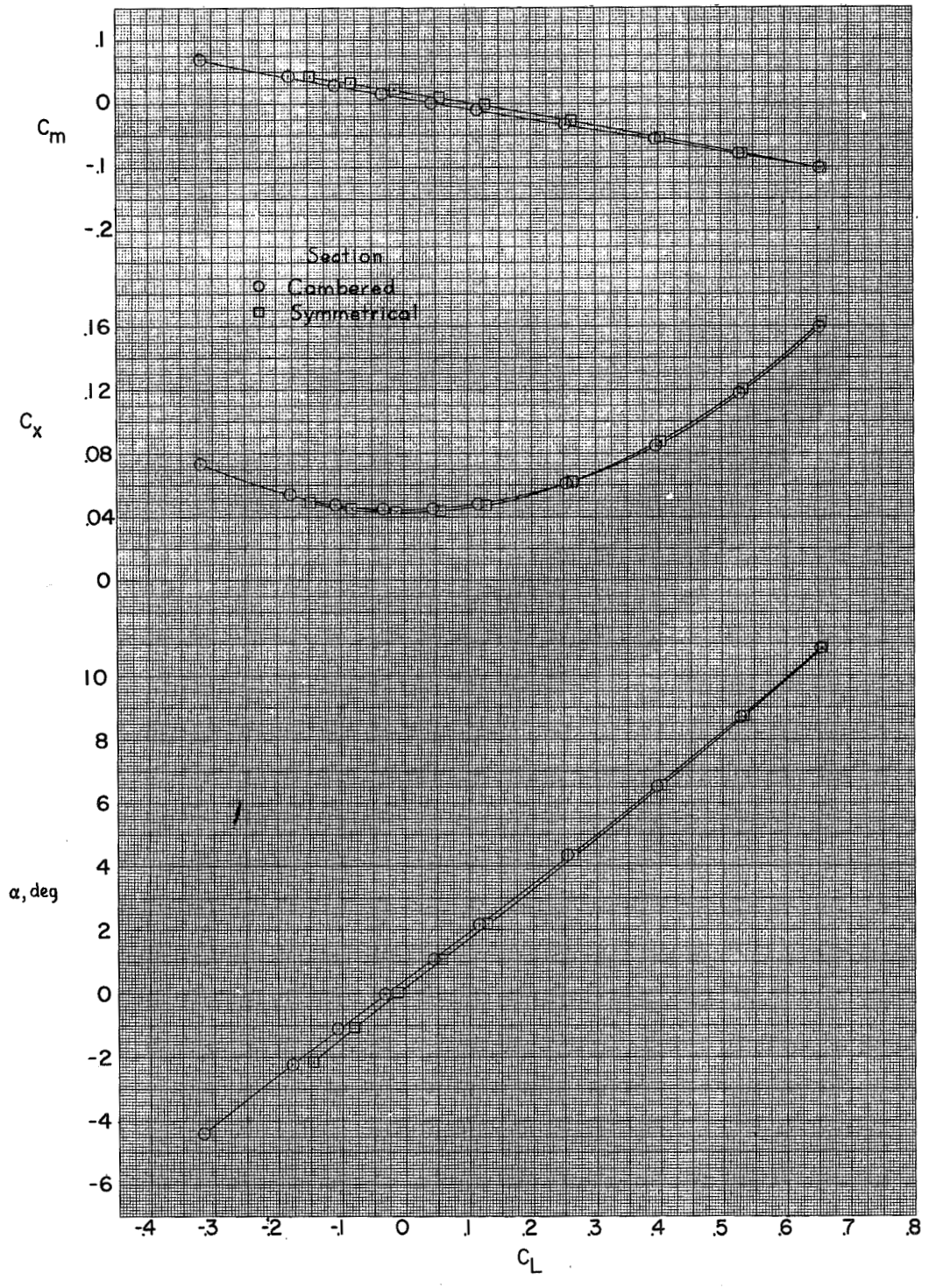

(a) Horizontal tail off.

Figure 9.- Effect of wing section on aerodynamic characteristics in pitch. Inlets open; $i_t = 0^\circ$.

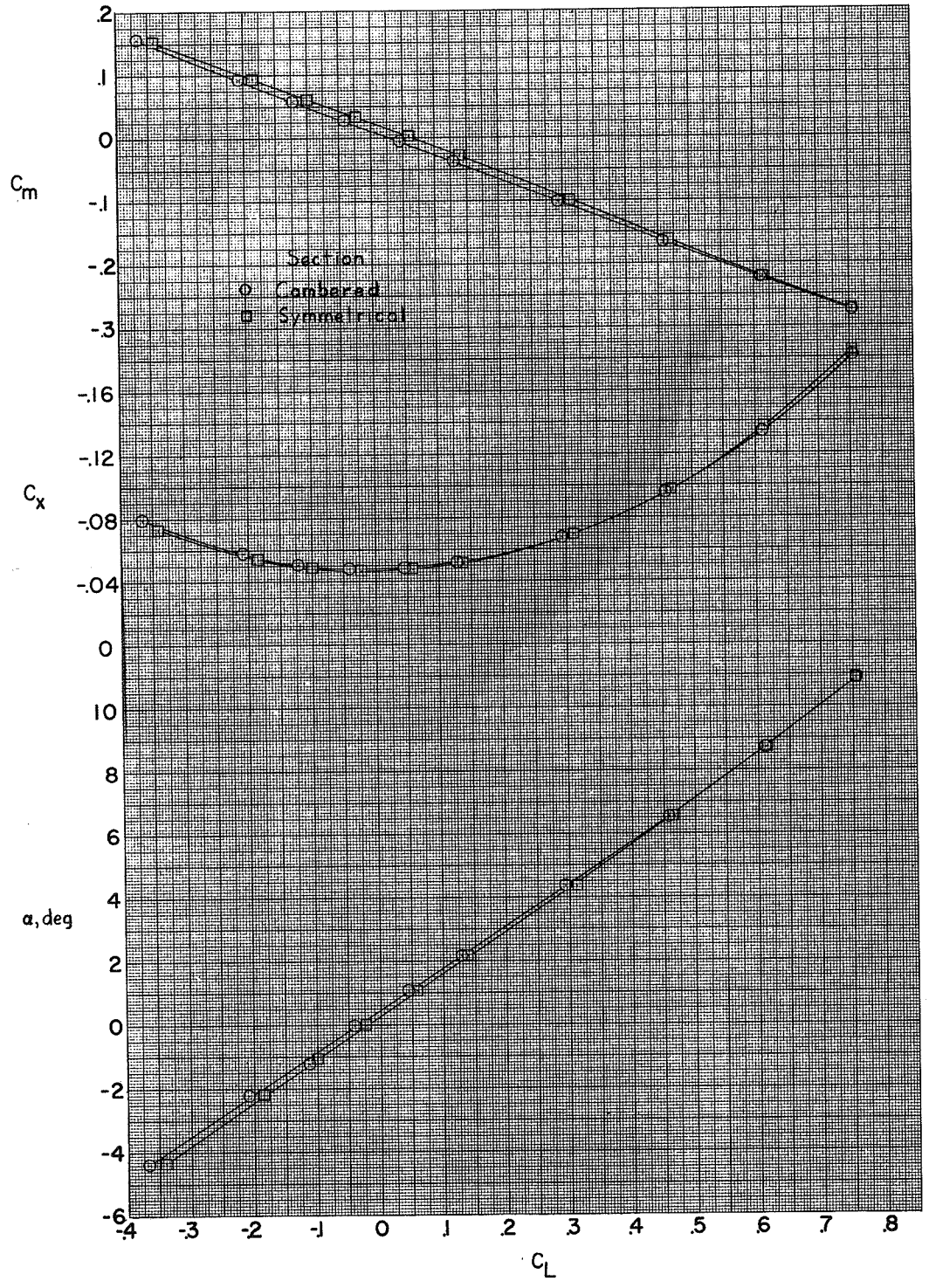

(b) Horizontal tail on.

Figure 9.- Concluded.

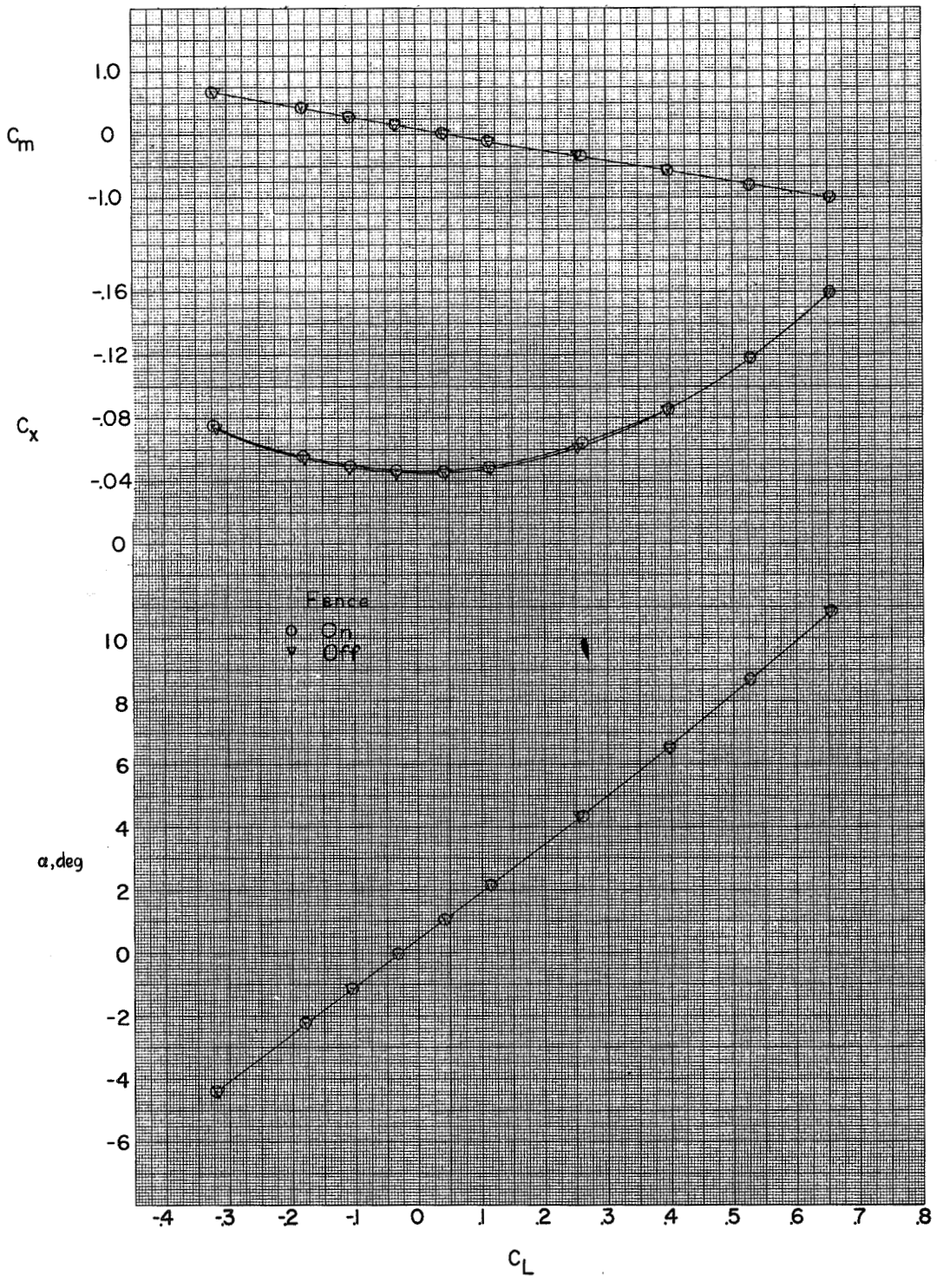

(a) Horizontal tail off.

Figure 10.- Effect of wing fences on aerodynamic characteristics in pitch. Configuration $W_C B_1 V$; inlets open.

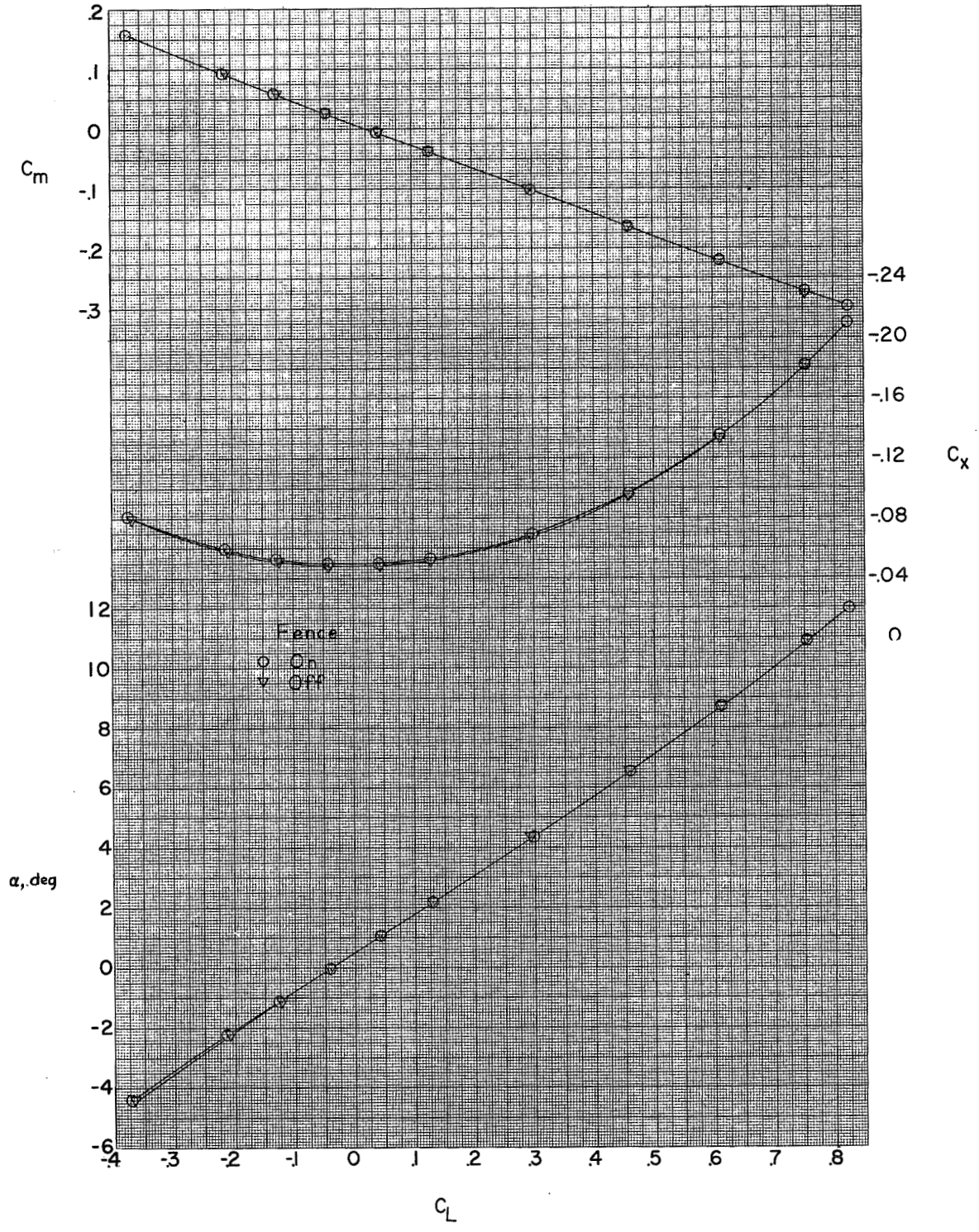

(b) Horizontal tail on; $i_t = 0^\circ$.

Figure 10.- Concluded.

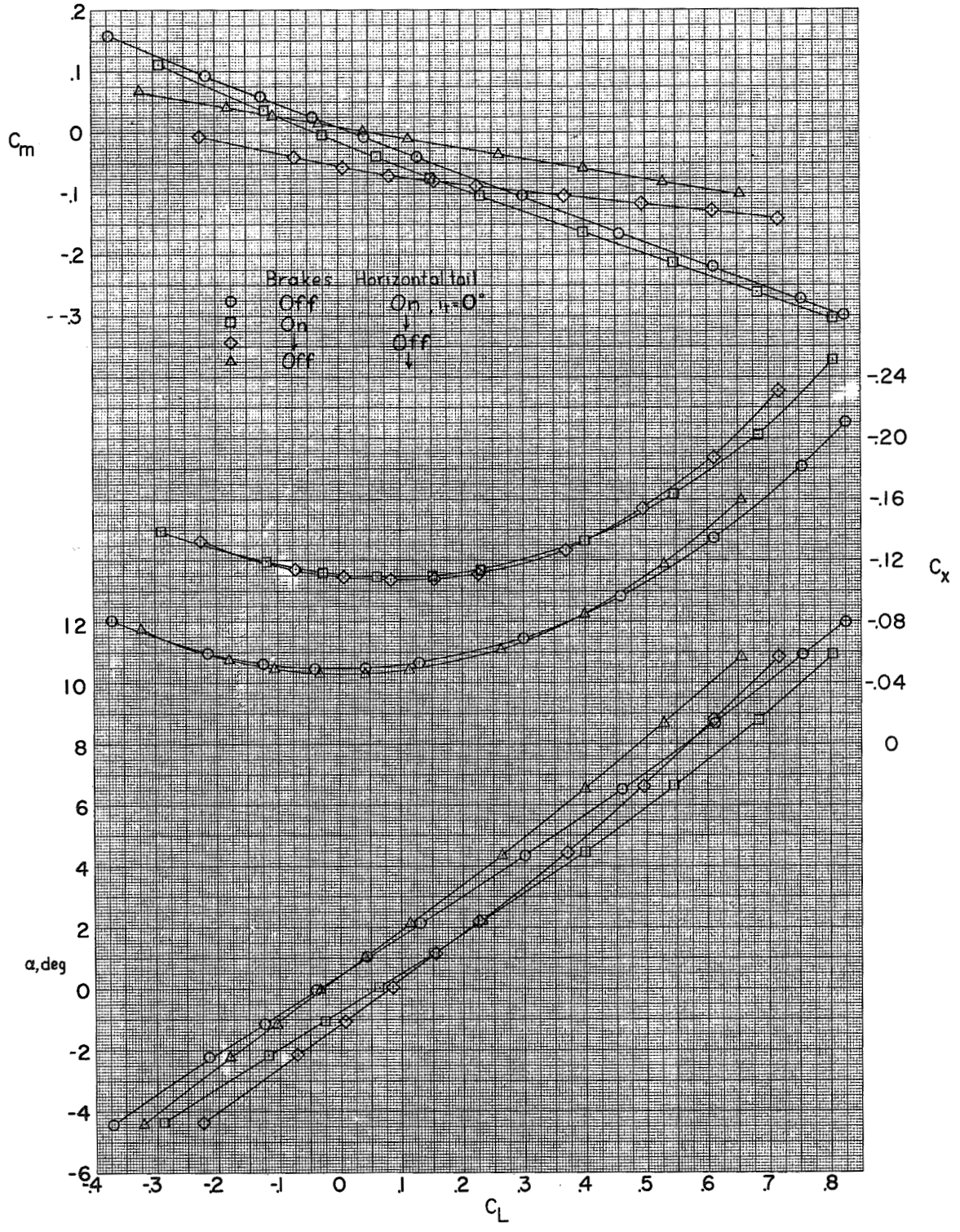

Figure 11.- Effect of dive brakes on aerodynamic characteristics in pitch. Configuration $W_C B_1 V$; inlet open.

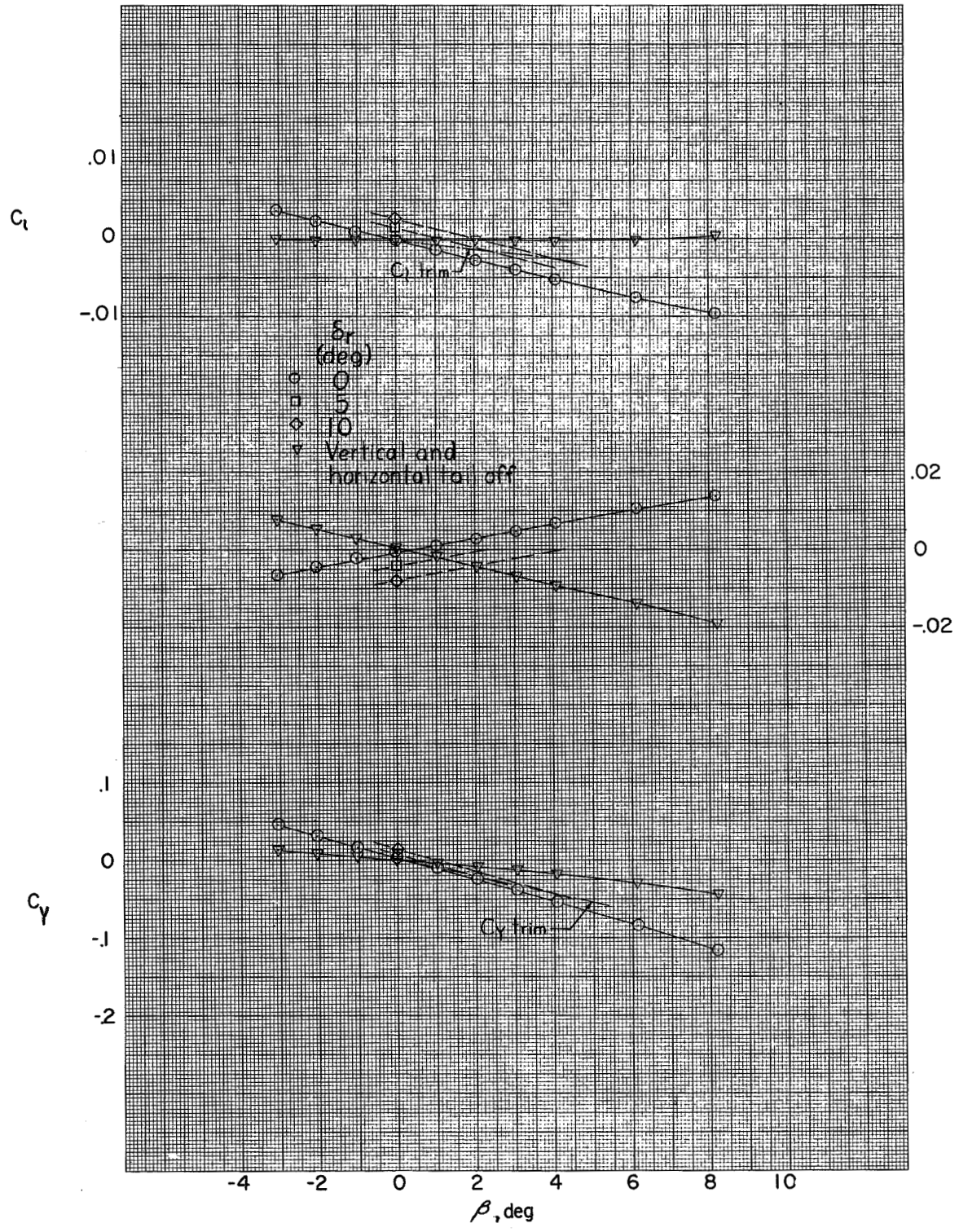

Figure 12.- Aerodynamic characteristics in sideslip. Inlets open; $\alpha \approx 0^\circ$; $i_t = 0^\circ$.

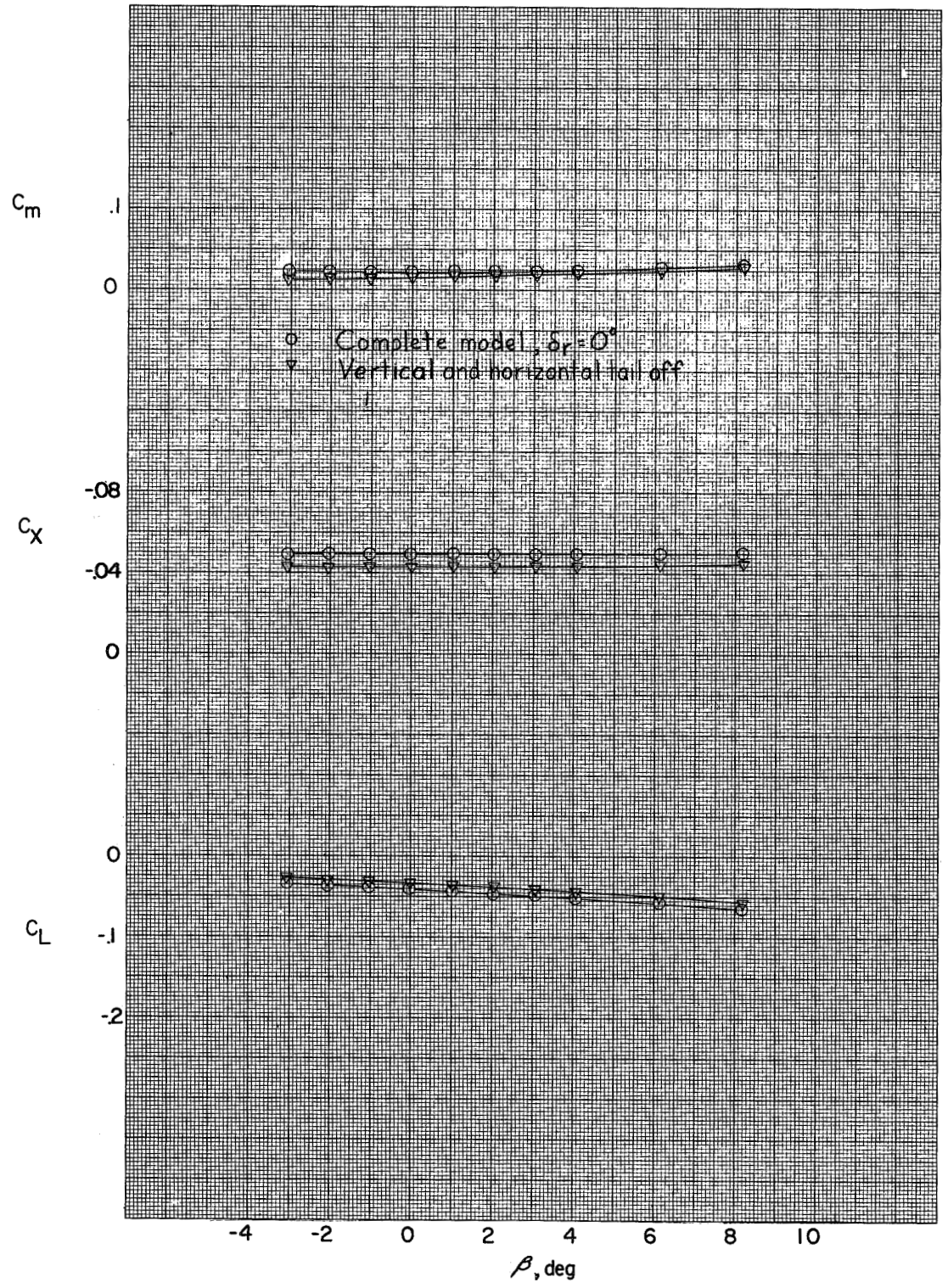

Figure 12.- Concluded.

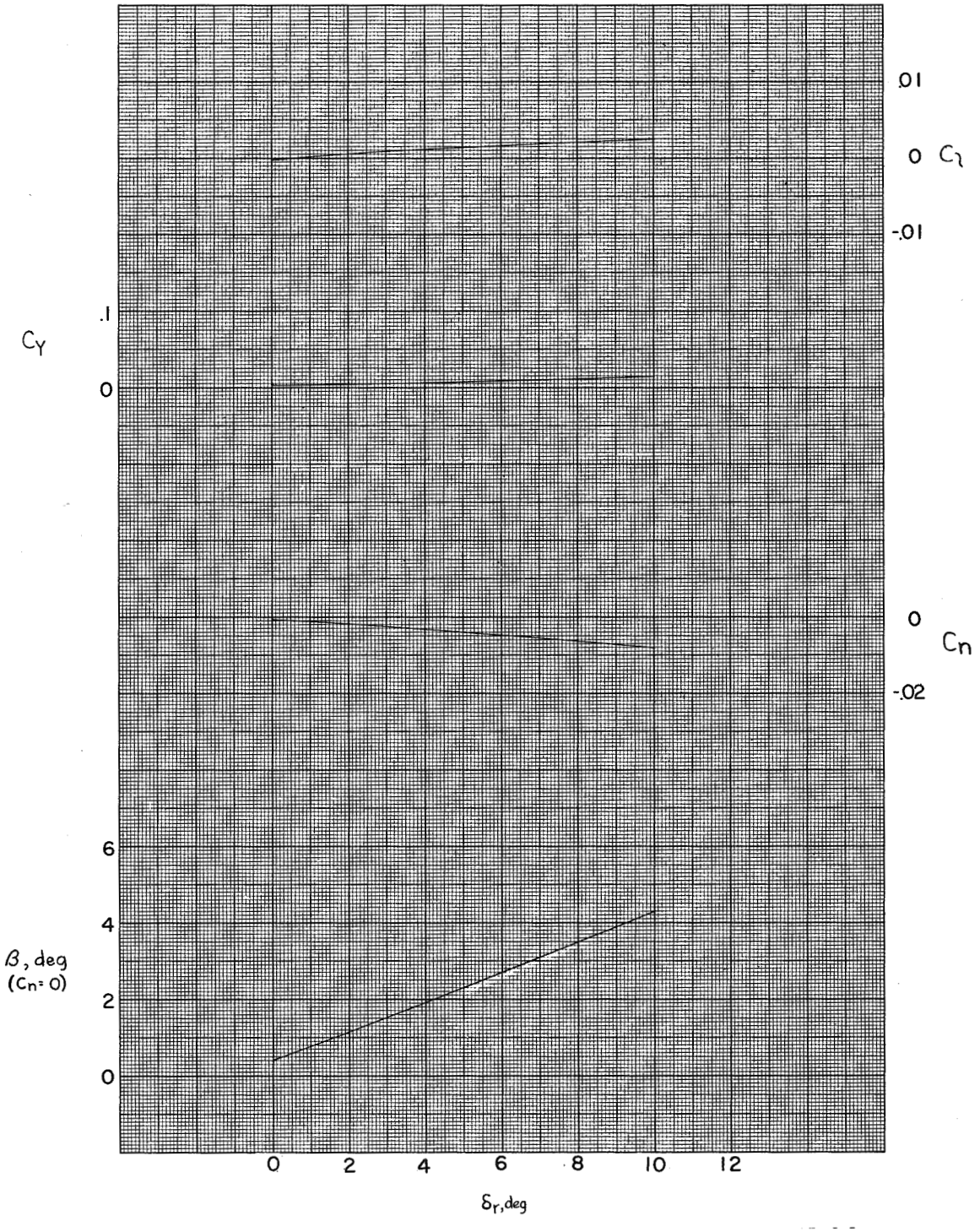

Figure 13.- Directional control characteristics. $\alpha = 0^{\circ}$.

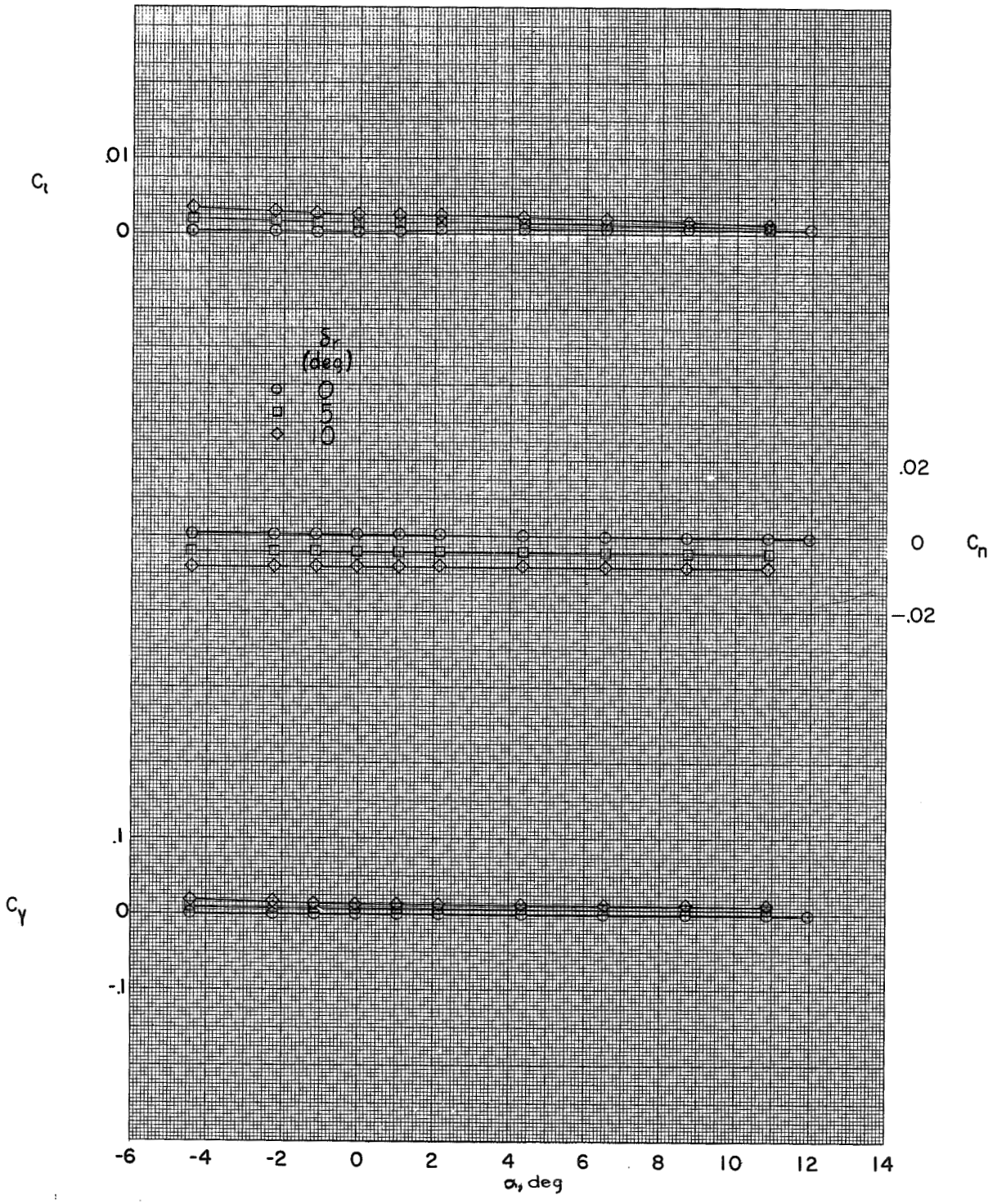

Figure 14.- Effect of angle of attack on directional control characteristics. Configuration $W_C B_1 ZVH$; inlets open; $\beta = 0^\circ$.